Supporting Information for:

Speciation of arsenic, chromium and vanadium in red mud samples from the Ajka spill site, Hungary.

Ian T. Burke[1*], William M. Mayes[2], Caroline L. Peacock[1], Andrew P. Brown[3], Adam P. Jarvis[4] and Katalin Gruiz[5].

[1] Earth Surface Science Institute, School of Earth and Environment, University of Leeds, Leeds LS2 9JT, UK.

[2] Centre for Environmental and Marine Sciences, University of Hull, Scarborough, YO11 3AZ, UK.

[3] School of Process, Environmental and Materials Engineering, University of Leeds, Leeds LS2 9JT, UK.

[4] School of Civil Engineering and Geosciences, Newcastle University, Newcastle upon Tyne, NE1 7RU, UK.

[4] Department of Applied Biotechnology and Food Science, Budapest University of Technology and Economics. 1111 Budapest, St. Gellért sq. 4. Hungary.

[*] Corresponding Author's E-mail: i.burke@see.leeds.ac.uk

This section consists of 11 pages, 3 tables, and 5 figures.

Section 1. XAS analysis.

Approximately 100mg samples of dried red mud samples K1a and K1c and the precipitate recovered from red mud leachate experiments were prepared for XAS analysis by vigorous homogenisation in an acid washed agate mortar and pestle and pressed into 8 mm pellets held in Kapton™ tape. Standard materials were also prepared as pressed pellets using cellulose as a diluent to reduce chemical thickness (to achieve an edge step between 0.5 and 1.5 in transmission mode, see below) and held in Kapton™ tape. Solutions of sodium arsenate and sodium arsenite were prepared at 1000 mg.L^{-1} and held in polythene bags for analysis. A sodium vanadate solution was prepared in 0.1 mol.L^{-1} NaOH, also at 1000 mg.L^{-1}, and held in polythene bags as above.

As, Cr and V K-edge spectra were collected on beamline I18 at the Diamond Light Source operating at 3 GeV with a typical current of 200 mA, using a nitrogen cooled Si(111) double crystal monochromator and focussing optics. A pair of plane mirrors was used to reduce the harmonic content of the beam and Kirkpatrick-Baez mirrors were used to produce a relatively unfocused beam (approximately 0.5mm diameter at the sample). For standards prepared as pressed pellets, K-edge spectra were collected in transmission mode at room temperature (~295 °K). For samples and solutions, data were collected in fluorescence mode using a 9 element solid state Ge detector at room temperature. As K-edge spectra were found to be strongly affected by beam damage presenting as an apparent change in As speciation that increased in magnitude with increased exposure to the beam. To mitigate this effect, only single As K-edge EXAFS spectra where collected (~25mins) from a spot within the sample and the sample stage automatically moved to expose an unaffected part of the sample before subsequent scans.

Cr K-edge spectra for the 5% Cr^{3+}-substituted hematite sample were collected at the SuperXAS beamline of the Swiss Light Source operating at 2.4 GeV with a typical current of 400 mA. Analysis was in transmission mode using a water cooled Si(111) double crystal monochromator and vertically collimating and Toroidal focusing mirrors.

Multiple scans were then averaged to improve the signal to noise ratio using Athena version 0.8.061 (Ravel and Newville, 2005). For XANES spectra absorption was also normalised in Athena over the full data range and plotted from approximately -15 eV to +30 eV relative to the edge

position with no correction required for drift in E_0. Cr and V data was calibrated using E_0 measured from thin metal foils, and As data was calibrated using the white line position measured from the sodium arsenate standard. The V pre-edge peak energy was determined by calculation of the area normalised centroid energy position following the method of Chaurand et al. (2007).

Section 2 As K-edge EXAFS Analysis.

EXAFS data was background subtracted using PySpline v1.1 (Tenderholt et al. 2007) and analysed in DLexcurv v1.0 (Tomic et al., 2005) using full curved wave theory (Gurman et al., 1984). Phaseshifts were derived from *ab initio* calculations using Hedin-Lundqvist potentials and von-Barth ground states (Binsted, 1998). Multiple scattering was allowed for as coded in DLexcurv (Binsted, 1998; Tomic et al., 2005). Multiple scattering calculations require specification of the full three dimensional structure of the As coordination environment (i.e., bond angles in addition to bond lengths). This was done using hypothetical model clusters with C_1 symmetry (SI Figure SI 1). The spectra for each sample were then fit by refining each model cluster, and the best fit evaluated using the EXAFS R-factor (Binsted et al., 1992), the EXAFS Fit Index (as coded in Binsted et al., 1996) and the reduced Chi^2 values (as coded in EXCURV98 (Binsted, 1998 and references therein)). Specifically, reduced Chi^2 values were used to evaluate the fits of each experimental spectrum to various single shell (involving only nearest neighbour oxygens) vs. multiple shell (involving nearest neighbour oxygens and next-nearest neighbour Al/Fe) model clusters. In this way the statistical significance of invoking Al/Fe backscatters was determined. Next-nearest neighbour Al/Fe shells were only included if the reduced Chi^2 was improved by $\geq$ 10%, compared to a single shell (oxygens only) cluster (Peacock, 2009). It should be noted that, in DLexcurv, the absolute value of reduced Chi^2 is not accurate (as DLexcurv does not require actual experimental statistical errors). Rather, reduced Chi^2 is used as a relative guide where a reduction or minimum indicates an improved fit. Fitting involved the refinement of an energy correction Ef (the Fermi Energy; which for final fits typically varied between ~ -6.5 and -7.5), and the absorber-scatterer distance and the Debye-Waller factor for each shell. The amplitude factor (or AFAC in DLexcurv V1.0) was retained as the default of 1 throughout. During fitting the number of independent data points was always greater than the number of fitted parameters (in DLexcurv these are N_{ind} and N_{pars}, respectively). N_{ind} was determined using Stern's rule

(Stern, 1993) as $2\Delta k\Delta R/\pi + 2$ (Booth and Hu, 2009) where Δk and ΔR are the range in k- and R-space actually fitted. All spectra were fit in k-space and no Fourier filtering was performed.

Fourier transforms of the EXAFS spectra were used to obtain an approximate radial distribution function around the central As atom (the absorber atom); the peaks of the Fourier transform can be related to "shells" of surrounding backscattering ions characterised by atom type, number of atoms, absorber-scatterer distance, and the Debye-Waller factor (± 25%), $2\sigma^2$. Atomic distances calculated by DLexcurv have an error of approximately ± 0.02 and ± 0.05 Å in the first and outer shells respectively (Burke et al., 2005). Debye-Waller factors are typically $0.002 - 0.02$ $2\sigma^2$ for the first shell and $0.02 - 0.04$ $2\sigma^2$ for the outer shells (Binsted, 1998).

Table SI 1. Composition of major and minor elements in K1 red mud sample replicates (mg.kg^{-1}) determined by ICP-OES/MS after total microwave assisted digestion in aqua regia-HF.

Element	K1a	K1b	K1c	K1 Mean	Std Dev
Al	65804	82677	75319	**74600**	*8460*
As	89	37	110	**79**	*38*
Au	24.8	20.8	25.8	**23.8**	*2.7*
Ba	80.2	64.3	67.2	**70.6**	*8.5*
Be	9.4	8.9	8.9	**9.1**	*0.3*
Ca	53765	50482	55708	**53318**	*2641*
Cd	5.9	2.9	3.3	**4.0**	*1.6*
Ce	426	409	378	**405**	*25*
Co	112	87	92	**97**	*13*
Cr	934	733	766	**811**	*108*
Cu	64.3	51.1	52.6	**56.0**	*7.3*
Er	22.2	17.6	17.0	**19.0**	*2.8*
Eu	8.5	6.2	5.3	**6.7**	*1.6*
Fe	213590	197528	214400	**208506**	*9516*
Ga	78.5	82.3	77.0	**79.3**	*2.7*
Gd	81.5	68.8	71.7	**74.0**	*6.7*
Ge	26.3	28.0	26.2	**26.8**	*1.0*
Hf	4.2	8.5	8.2	**7.0**	*2.4*
Hf	14.8	13.9	14.0	**14.3**	*0.5*
Ho	10.2	9.0	8.7	**9.3**	*0.8*
K	796	730	685	**737**	*56*
La	183	141	124	**149**	*30*
Li	57.6	58.2	56.8	**57.5**	*0.7*
Lu	8.8	7.8	9.5	**8.7**	*0.9*
Mg	3159	2760	3028	**2982**	*203*
Mn	3055	2294	2349	**2566**	*425*
Mo	18.0	13.3	11.9	**14.4**	*3.2*
Na	42226	40372	37157	**39918**	*2565*
Nb	97.2	76.5	79.7	**84.5**	*11.2*
Nd	167	122	112	**133**	*29*
Ni	388	289	286	**321**	*58*
P	1262	1035	1086	**1128**	*119*
Pb	179	140	152	**157**	*20*
Pr	121	102	97	**107**	*13*
Pt	78.6	58.6	76.7	**71.3**	*11.0*
Ru	44.5	30.7	29.7	**35.0**	*8.3*
S	2894	2886	2751	**2844**	*81*
Si	30012	29369	25543	**28308**	*2416*
Sm	37.5	26.1	24.2	**29.3**	*7.2*
Sr	273	240	244	**252**	*18*
Te	17.1	15.4	24.4	**19.0**	*4.8*
Th	127	129	129	**128**	*1*
Ti	25878	24086	24040	**24668**	*1048*
Tm	9.8	9.1	8.8	**9.2**	*0.5*
U	369	314	333	**339**	*28*
V	963	860	897	**907**	*52*
Y	114	82	74	**90**	*21*
Yb	19.0	15.6	15.1	**16.6**	*2.1*
Zn	218	143	158	**173**	*40*
Zr	653	619	615	**629**	*21*

Table SI 2. Hydrochemical composition of red mud leachate collected at dyke breach location K1 on 1st December 2010 (0.45 μm filtered; see Mayes et al., 2011 for details of analytical methods).

Determinand	K1 red mud leachate
pH	13.1
ORP (V)	0.023
Temperature (^oC)	3.6
Selected ions / elements (mg L^{-1})	
Alkalinity (as OH^-)	1125.8
Alkalinity (as CO_3^{2-})	2445.8
Alkalinity (as HCO_3^-)	1.4
Al	659
As	3.612
B	0.900
Ca	1.3
Chloride	83
Cr	0.049
Cu	0.310
Fe	<0.001
Ga	2.340
K	85
Mg	0.001
Mo	4.114
Na	701
Ni	0.036
Pb	<0.001
Si	0.668
Sulphate	727
V	5.709

< less than given limit of detection

SI Table SI 3. Mineral saturation indexes based on the water composition determined at location K1 (SI Table SI 2). Results based on PHREEQC modelling using MINTEQ (Cr and V phases), Bothe and Brown, 1999 (Ca-arsenate hydrate phases) and WATEQ4F (all other phases).

Saturation Index

Phase	Species	Sat. Index	As phases	Species	Sat. Index
Adularia	$KAlSi_3O_8$	**2.61**	$Ca_5(AsO_4)_3OH$	$Ca_5(AsO_4)_3OH$	-80.08
Al(OH)$_3$(a)	$Al(OH)_3$	**1.39**	$CaHAsO_4.H_2O$	$CaHAsO_4.H_2O$	-28.08
Albite	$NaAlSi_3O_8$	**0.9**	Ferrarisite	$Ca_5H_2(AsO_4)_4.9H_2O$	-103.34
Alunite	$KAl3(SO_4)2(OH)_6$	**2.76**	Guerinite	$Ca_5H_2(AsO_4)_4.9H_2O$	-102.54
Analcime	$NaAlSi_2O_6:H_2O$	**0.25**	Claudetite	As_4O_6	-162.4
Anorthite	$CaAl_2Si_2O_8$	**1.44**	$Ni_3(AsO_4)_2:8H_2O$	$Ni_3(AsO_4)_2:8H_2O$	-32.1
Aragonite	$CaCO_3$	**0.4**	Orpiment	As_2S_3	-452.3
Artinite	$MgCO_3:Mg(OH)_2:3H_2O$	-10.54	Realgar	AsS	-184.2
Barite	$BaSO_4$	-0.98			
Basaluminite	$Al_4(OH)10SO_4$	**10.17**	**Cr phases**		
Boehmite	AlOOH	**3.51**	$BaCrO_4$	$BaCrO_4$	-3.20
Brucite	$Mg(OH)_2$	-7.11	$CaCrO_4$	$CaCrO_4$	-10.6
Calcite	$CaCO_3$	**0.56**	$Cr(OH)_3$	$Cr(OH)_3$	-16.7
Chlorite14A	$Mg_5Al_2Si_3O_{10}(OH)_8$	-8.49	Cr_2O_3	Cr_2O_3	-32.1
Chlorite7A	$Mg_5Al_2Si_3O_{10}(OH)_8$	-12.07	$CrCl_2$	$CrCl_2$	-82.8
Chrysotile	$Mg_3Si_2O_5(OH)_4$	-11.41	$CrCl_3$	$CrCl_3$	-80.3
Clinoenstatite	$MgSiO_3$	-6.29	CrF_3	CrF_3	-60.7
CuMetal	Cu	**0.46**	CrMetal	CrMetal	-106.5
Cuprite	Cu_2O	**3.48**	CrO_3	CrO_3	-29.9
Diaspore	AlOOH	**5.41**	Li_2CrO_4	Li_2CrO_4	-23.32
Diopside	$CaMgSi_2O_6$	-6.61	$MgCr_2O_4$	$MgCr_2O_4$	-27.7
Dolomite	$CaMg(CO_3)_2$	-1.85	$MgCrO_4$	$MgCrO_4$	-18.3
Dolomite(d)	$CaMg(CO_3)_2$	-2.50	$Na_2Cr_2O_7$	$Na_2Cr_2O_7$	-33.6
Forsterite	Mg_2SiO_4	-13.60	Na_2CrO_4	Na_2CrO_4	-14.2
Gibbsite	$Al(OH)_3$	**4.29**	$SrCrO_4$	$SrCrO_4$	-10.51
Halloysite	$Al_2Si_2O_5(OH)_4$	**2.46**			
Hausmannite	Mn_3O_4	-18.99	**V phases**		
Huntite	$CaMg_3(CO_3)_4$	-11.05	$Ca_2V_2O_7$	$Ca_2V_2O_7$	-4.48
Hydroxyapatite	$Ca_5(PO_4)3OH$	-2.17	$Ca_3(VO_4)_2$	$Ca_3(VO_4)_2$	-5.82
Kaolinite	$Al_2Si_2O_5(OH)_4$	**7.79**	Ca-vanadate	$Ca_{0.5}VO_3$	-8.35
Kmica	$KAl_3Si_3O_{10}(OH)_2$	**16.69**	$Mg_2V_2O_7$	$Mg_2V_2O_7$	-11.09
Laumontite	$CaAl_2Si_4O_{12}:4H_2O$	**4.11**	Na_3VO_4	Na_3VO_4	-20.97
Leonhardite	$Ca_2Al_4Si_8O_{24}:7H_2O$	**16.68**	$Na_4V_2O_7$	$Na_4V_2O_7$	-12.82
Magnesite	$MgCO_3$	-2.90	Na-vanadate	$NaVO_3$	-8.11
Ni(OH)$_2$	$Ni(OH)_2$	-3.05	$V(OH)_3$	$V(OH)_3$	-36.12
Phlogopite	$KMg_3AlSi_3O_{10}(OH)_2$	-6.52	V_2O_3	V_2O_3	-34.5
Plumbogummite	$PbAl_3(PO_4)_2(OH)_5:H_2O$	**4.67**	V_2O_4	V_2O_4	-20.9
Prehnite	$Ca_2Al_2Si_3O_{10}(OH)_2$	**2.29**	V_2O_5	V_2O_5	-14.8
Pyrophyllite	$Al_2Si_4O_{10}(OH)_2$	**5.21**	V_3O_5	V_3O_5	-89.0
Sepiolite	$Mg_2Si_3O7.5OH:3H_2O$	-9.08	V_4O_7	V_4O_7	-111.0
Sepiolite(d)	$Mg_2Si_3O7.5OH:3H_2O$	-11.37	V_6O_{13}	V_6O_{13}	-103.6
Strontianite	$SrCO_3$	-1.40	VCl_2	VCl_2	-99.5
Talc	$Mg_3Si_4O_{10}(OH)_2$	-10.55	VCl_3	VCl_3	-100.5
Tremolite	$Ca_2Mg_5Si_8O_2(OH)_2$	-18.35	VF_4	VF_4	-108.5
Witherite	$BaCO_3$	-0.04	VMetal	VMetal	-131.9
			VO	VO	-62.3
As phases			$VO(OH)_2$	$VO(OH)_2$	-21.7
$AlAsO_4:H_2O$	$AlAsO_4:H_2O$	-18.45	VO_2Cl	VO_2Cl	-34.5
Arsenolite	As_4O_6	-162.6	VOCl	VOCl	-55.3
As_2O_5	As_2O_5	-54.62	$VOCl_2$	$VOCl_2$	-62.1
$Ba_3(AsO_4)_2$	$Ba_3(AsO_4)_2$	**9.94**	$VOSO_{4(C)}$	$VOSO_{4(C)}$	-49.8
$Ca_3(AsO4)_2:4H_2O$	$Ca_3(AsO4)_2:4H_2O$	-8.63			
$Ca_3(AsO_4).4¼H_2O$	$Ca_3(AsO_4).4¼H_2O$	-5.82			
$Ca_3(AsO_4).3⅔H_2O$	$Ca_3(AsO_4).3⅔H_2O$	-46.28			
$Ca_4(OH)_2(AsO_4)_2.4H_2O$	$Ca_4(OH)_2(AsO_4)_2.4H_2O$	-62.73			

a)

b)
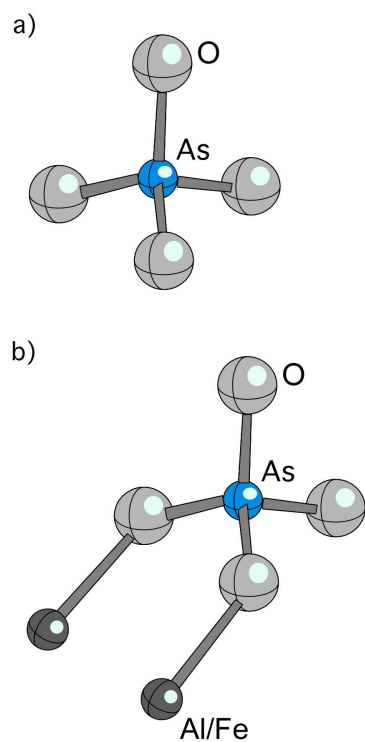
Figure SI 1. Clusters used to model As EXAFS data of (a) dried red mud samples K1a and K1c, and (b) the precipitate recovered from the red mud leachate experiments. As = arsenic; O = oxygen; Al = aluminium; Fe = iron.
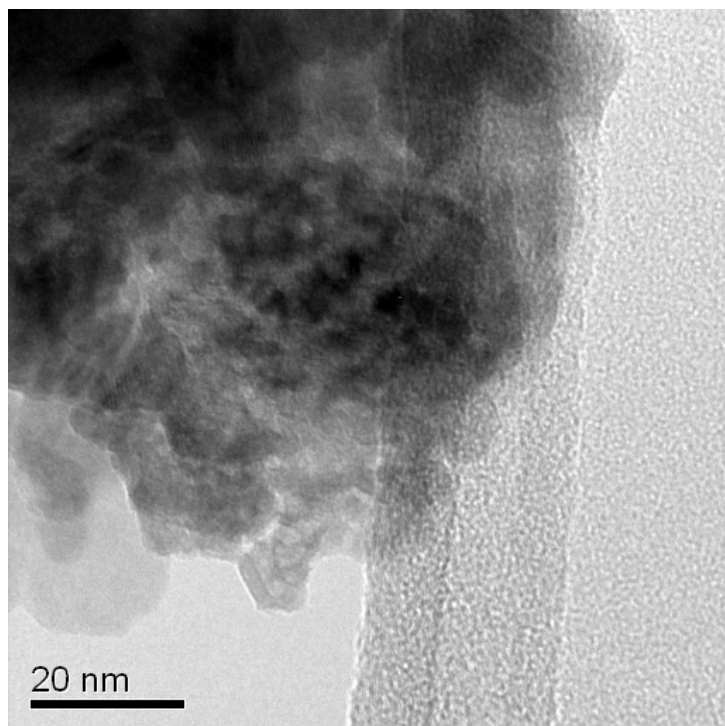
Figure SI 2. High resolution bright field TEM image of fine grained hematite particles.
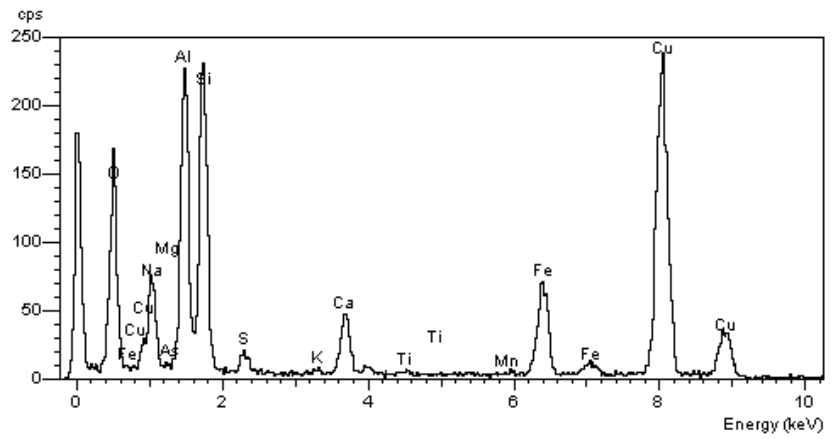
Figure SI 3. TEM image and EDX spectra from a larger plate like mineral (centre) containing a Na-Al-Si composition consistent with a cancrinite-like phase. V peaks were never found associated with particles with a similar composition. Cu peaks are from the support grid used to mount samples.
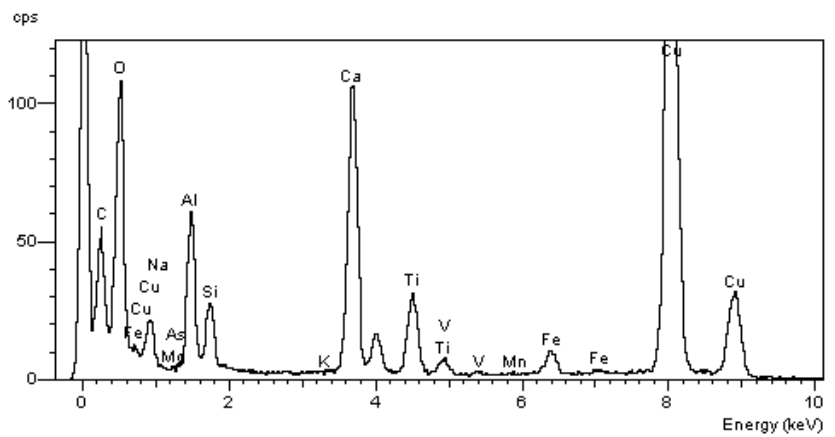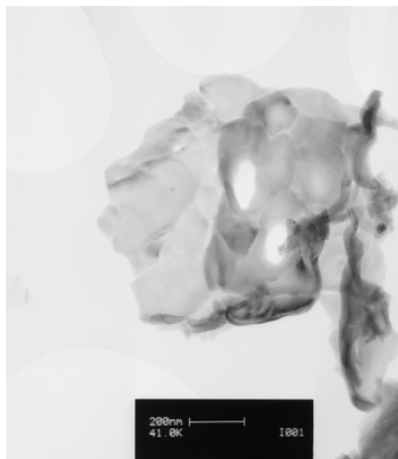
Figure SI 4. TEM image and EDX spectra from a larger plate like mineral containing Ca-Al-Si-Ti composition consistent with a hydrogarnet-like phase. V peaks were identified in EDS spectra from particles with a similar composition. Cu and C peaks are from the Cu-support grid and C-film used to mount samples.
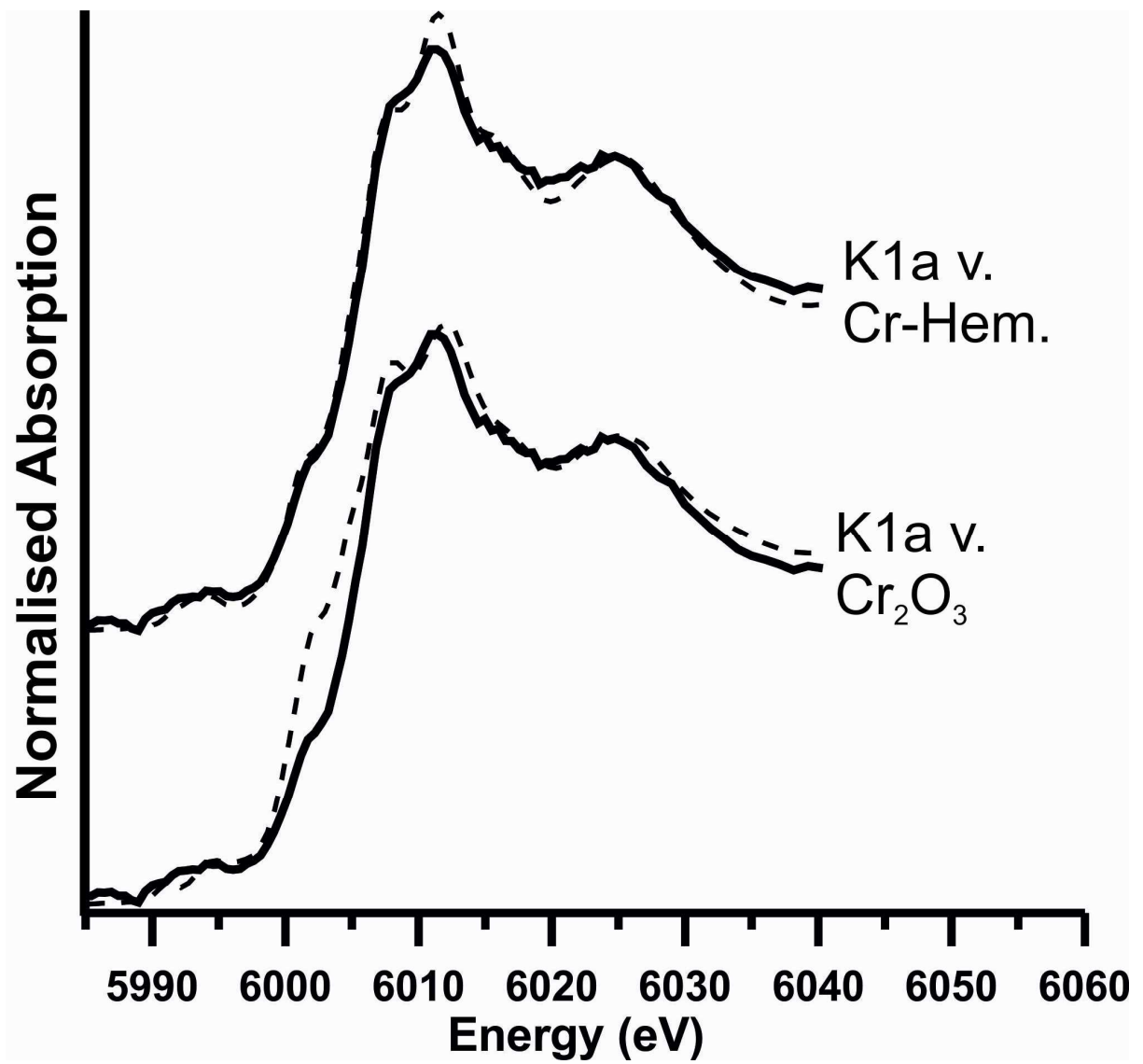
Figure SI 5. Detailed comparison of the Cr K-edge XANES spectra collected from the K1a red mud sample (solid lines) and spectra collected from a 5 % Cr(III)-substituted hematite (top) and Cr2O3 (bottom) standards (dashed lines).

Supporting Information References

N. Binsted, CLRC Daresbury Laboratory EXCURV98 program, CLRC Daresbury Laboratory, Warrington, UK, 1998.

N. Binsted, R.W. Strange, S.S. Hasnain, Constrained and Restrained Refinement in Exafs Data-Analysis with Curved Wave Theory, Biochemistry, 31 (1992) 12117-12125.

Booth, C. H.; Hu, Y. J., Confirmation of standard error analysis techniques applied to EXAFS using simulations. In 14th International Conference on X-Ray Absorption Fine Structure, DiCicco, A.; Filipponi, A., Eds. Iop Publishing Ltd: Bristol, 2009; Vol. 190.

Bothe, J.V., Brown, P.W., The stabilities of calcium arsenates at 23 ± 1 $^\circ$C. Journal of Hazardous Materials. 1999, B69, 197-207.

I.T. Burke, C. Boothman, J.R. Lloyd, R.J.G. Mortimer, F.R. Livens, K. Morris, Effects of progressive anoxia on the solubility of technetium in sediments, Environ. Sci. Technol., 39 (2005) 4109-4116.

Chaurand, P.; Rose, J.; Briois, V.; Salome, M.; Proux, O.; Nassif, V.; Olivi, L.; Susini, J.; Hazemann, J.-L.; Bottero, J.-Y., New methodological approach for the vanadium K-edge X-ray absorption near-edge structure interpretation: Application to the speciation of vanadium in oxide phases from steel slag. Journal of Physical Chemistry B 2007, 111, (19), 5101-5110.

S.J. Gurman, N. Binsted, I. Ross, A Rapid, Exact Curved-Wave Theory for Exafs Calculations, Journal of Physics C-Solid State Physics, 17 (1984) 143-151.

Mayes, W. M.; Jarvis, A. P.; Burke, I. T.; Walton, M.; Feigl, V.; Klebercz, O.; Gruiz, K., Dispersal and Attenuation of Trace Contaminants Downstream of the Ajka Bauxite Residue (Red Mud) Depository Failure, Hungary. *Environmental Science & Technology* **2011,** *45*, (12), 5147-5155.

C. Peacock, Physiochemical controls on the crystal-chemistry of Ni in birnessite: Genetic implications for ferromanganese precipitates, Geochim. Cosmochim. Acta 73 (2009) 3568-3578.

B. Ravel, M. Newville, ATHENA, ARTEMIS, HEPHAESTUS: data analysis for X-ray absorption spectroscopy using IFEFFIT, J. Synchrot. Radiat., 12 (2005) 537-541.

A. Tenderholt, B. Hedman, K.O. Hodgson, PySpline: A modern, cross-platform program for the processing of raw averaged XAS edge and EXAFS data, in: B. Hedman, P. Painetta (Eds.) X-Ray Absorption Fine Structure-XAFS13, 2007, pp. 105-107.

S. Tomic, B.G. Searle, A. Wander, N.M. Harrison, A.J. Dent, J.F.W. Mosselmans, J.E. Inglesfield, CCLRC Technical Report DL-TR-2005-001, ISSN 1362-0207(2005), in, 2005.

Stern, E. A., number of relevant independent points in x-ray-absorption fine-structure spectra. Physical Review B 1993, 48, (13), 9825-9827.